

Article

Numerical Simulation of PMMA Impact Based on the J–C Constitutive and Damage Models under Hydrostatic Pressure Loading

Qinghai Du *, Fengyou Liu and Qi Lei

School of Engineering, Shanghai Engineering Research Center of Hadal Science and Technology, Shanghai Ocean University, Shanghai 201306, China

* Correspondence: qhdu@shou.edu.cn; Tel.: +86-21-61900730

Abstract: Polymethyl methacrylate (PMMA) polymer is widely used in various fields today. In order to reveal the structural impact performance of PMMA materials in underwater engineering thoroughly, this paper firstly proposed a simplified plate model for a spherical shell hull under concentrative impact loading. Then, to simulate the hyper-elastic material properties of PMMA in the impact process, the Johnson–Cook constitutive model and damage failure model were adopted. And the least squares method was used to confirm accurately the J–C constitutive and damage failure model parameters of PMMA through material test data. Moreover, the dynamic process of the steel bullet impacting the PMMA plate structure was analyzed by the finite element software ABAQUS. The calculation results show that the numerical simulation results in this paper have a good convergence, and the residual velocities at different initial velocities and thicknesses of plates are in good agreement with the experimental test data. Therefore, the feasibility and accuracy of the impact analysis of PMMA structures based on J–C constitutive and damage failure models in this paper are verified accordingly. Finally, based on the presented finite element model, the structure response and the variation of residual velocity of the bullet with the PMMA plate thickness was analyzed in depth; that is, the results show that the residual velocity of the bullet has a certain linear relationship with the thickness, even in an underwater environment, and even in an underwater environment will increase both with a thicker structure or a higher pressure.

Keywords: PMMA; J–C constitutive model; impact; loss and damage; numerical simulation



Citation: Du, Q.; Liu, F.; Lei, Q. Numerical Simulation of PMMA Impact Based on the J–C Constitutive and Damage Models under Hydrostatic Pressure Loading. *Appl. Sci.* **2023**, *13*, 8640. <https://doi.org/10.3390/app13158640>

Academic Editor: Abílio M.P. De Jesus

Received: 3 July 2023
Revised: 21 July 2023
Accepted: 25 July 2023
Published: 27 July 2023



Copyright: © 2023 by the authors. Licensee MDPI, Basel, Switzerland. This article is an open access article distributed under the terms and conditions of the Creative Commons Attribution (CC BY) license (<https://creativecommons.org/licenses/by/4.0/>).

1. Introduction

As a thermoplastic polymer, PMMA has good mechanical properties such as anti-aging, light weight, high transparency, and impact resistance. With today's rapidly developing technology, and the speed of ocean development and aviation exploration, it is widely used in various fields such as mechanical manufacturing, construction, aviation, and biomedical applications [1]. Currently, ocean exploration and the development of deep-sea equipment are receiving increasing attention from countries around the world, and have become a key development focus in the deep-sea field. For deep-sea equipment, transparent structures are increasingly being applied to meet the current multifunctional development needs of deep-sea vehicles [2]. As important components of deep submersibles, such as transparent cabins or observation windows, structural design calculation methods for their strength or fatigue life are currently mainly based on theory, and numerical or experimental research [3–6]. In the complex marine environment and the current situation of ocean competition among countries around the world, collisions and impacts of deep-sea equipment are inevitable.

In impact analysis, the material properties of collision structures have a significant effect on the impact process and results, such as the constitutive model and damage model characteristics of materials. The Johnson–Cook constitutive model and damage failure model [7] are theoretical methods proposed by two scholars, Johnson and Cook, in the

1980s and used widely in the field of impact collision. The authors conducted tensile and torsional tests on twelve kinds of materials at different strain rates and temperatures, and determined the J–C constitutive model parameters of these materials through numerical simulation and comparison of experimental results. Moreover, they proposed a fracture criterion that considers the effects of a large strain, high temperature, and high stress, and verified it through Taylor impact tests and numerical simulations. In the application of the J–C model, Liu [8], for example, expressed the physical constitutive equation of normalized 50SiMnVB steel according to the J–C model, and the strain rate range was from quasi-static to dynamic. Guo [9] modified the temperature softening term in the J–C constitutive model based on experimental results and proposed a modified J–C constitutive model for Q235 steel. For PMMA materials, Yu [10] studied the dynamic mechanical properties of PMMA at room temperature based on SHPB experiments. Yao [11] conducted compression experiments on organic glass specimens under quasi-static and impact conditions using an INSTRON electronic universal testing machine and a separate Hopkinson compression rod device. Wang [12] obtained the constitutive relationship of organic glass by studying the effect of temperature on the quasi-static tensile mechanical properties of organic glass thick plates, using the nonlinear elastic partial expression of the ZWT model. Paul Moy [13] et al. studied the room temperature uniaxial compression strain-rate response of PMMA in the strain rate range of $0.0001 \text{ s}^{-1} \sim 4300 \text{ s}^{-1}$.

With regards to the impacting problem, many researchers have focused on it in history. Kazarinov [14] conducted experimental research on the velocity of PMMA thin plates under high-speed steel projectile penetration using LS-DYNA. Wu [15] conducted experimental studies on the quasi-static and medium-strain-rate uniaxial tensile mechanical properties of PMMA using the MTS810 testing machine and the self-developed medium-strain-rate material-testing machine. For the damage behavior of the J–C failure model, Chen [16] conducted quasi-static material mechanical property experiments and tensile SHPB experiments on 45 steel under different stress states and temperatures, and determined the parameters of the J–C failure model throughout experimental data. Shash and Zuzov [17] simulated and studied the penetration process of different bullets in three kinds of aluminum plates with a modified constitutive J–C relationship and Cockcroft–Latham fracture criterion. Zeng [18] conducted an experimental study on the nonlinear mechanical properties of PMMA under uniaxial tension based on the theory of damage mechanics, and proposed an improved Maxwell model that can describe the strain-rate dependent and viscoelastic damage behavior of PMMA to reveal the impact resistance of PMMA materials. It is noted that experimental and preliminary numerical methods [19–23] have been proposed to study dynamic response of PMMA under quasi-static and dynamic loadings, such as different temperatures or tensile or compressive forces.

Therefore, this article aims to study the structural performance of underwater transparent pressure-resistant shells under impact, focusing on numerical simulation models based on J–C constitutive and damage models. The J–C constitutive and damage models of PMMA materials are determined by material specimen test data and the least squares method, and verified through PMMA plate specimen impact tests. Finally, the impact performance of pressure-resistant structures under static water pressure under impact is revealed.

2. Problem and Structural Modeling

In underwater engineering, especially in deep-sea engineering, due to the advantages of uniform force distribution, spherical structures are one of the most commonly used pressure-resistant hulls, as shown in Figure 1 (bottom).

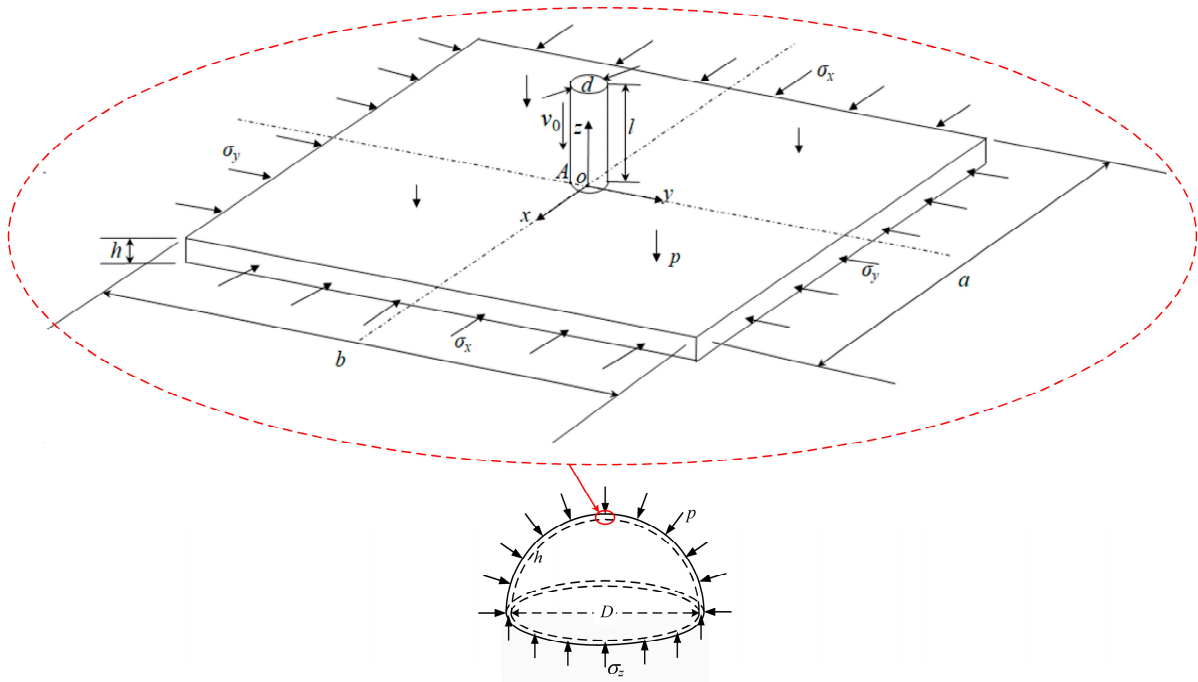


Figure 1. Simplified diagram of deep-sea impact model.

In order to simplify the impact problem of spherical shells for research purposes, this article will focus on the dynamic situation of concentrated impact loading onto the spherical shell, where the size of the impact body (projectile) is relatively far smaller compared with the spherical hull size. Therefore, according to the theory of plate and shell [24], in the local size region, the spherical shell surface could be simplified as a relatively flat plate. Then, the spherical shell under concentrative impact loading could be reduced to the plate structure impacted by a projectile. Thus, the proposed structural model is shown in Figure 1 (top).

The meanings of various structural parameter variables are defined, respectively, as: in Figure 1 (bottom), D is the diameter of the sphere, h is the thickness of the sphere, p is the acting external pressure, and σ is the internal stress under loading. In Figure 1 (top), a and b are the lengths of the blocks in the x and y directions (the coordinate system is shown in figure) respectively, while h is the thickness of the block, which is equal to the thickness of the sphere. Moreover, σ_x and σ_y are the internal stresses of the plate in two axis directions under acting pressure p , and d and l are the diameter and length of the steel bullet, respectively, with initial velocity v_0 .

3. J–C Constitutive Model and Damage Failure Model

Generally, in finite element collision simulation analysis, different models are used for the constitutive and damage models of PMMA [18,19], while Johnson and Cook explored the unity of material constitutive and damage models.

3.1. J–C Constitutive Model

The Johnson–Cook constitutive model focuses on describing the nonlinear stress–strain relationship of materials entering hyper elasticity, and the specific expression is as follows [2]

$$\sigma = (A + B\epsilon^n) \left(1 + C \ln \dot{\epsilon}^*\right) \left(1 - (T^*)^m\right) \tag{1}$$

In the formula, σ is the stress; ϵ is the plastic strain; $\dot{\epsilon}$ represents the strain rate; and T^* represents the relative dimensionless temperature parameter at the current temperature ($T^* = (T - T_r)/(T_m - T_r)$), where T_r is the room temperature and T_m is the reference temperature. The physical meaning of each parameter is: A represents the yield strength of the material; B and n represent material strain-strengthening parameters; C represents

the empirical strain-rate sensitivity coefficient; and m represents the temperature-softening effect. It is the reference strain rate of the constitutive model, usually taken as the strain rate of 10^{-3} s^{-1} in the quasi-static state.

When the temperature effect is not considered, the temperature remains at room temperature; that is, at this point, Equation (1) of the J–C model will become

$$\sigma = (A + B\varepsilon^n) \left(1 + C \ln \dot{\varepsilon}^*\right) \quad (2)$$

Based on the tensile/compressive test data of materials under different strains at room temperature, the least squares method can be used to determine the parameters of the J–C constitutive model of materials at room temperature. Under room temperature conditions, the values of A , B , and n are determined based on the curves obtained from material compression/tensile tests at strain rates. At this point, Equation (2) becomes

$$\sigma = A + B\varepsilon^n \quad (3)$$

Take the logarithm of both ends of Equation (3), with

$$\ln(\sigma - A) = \ln B + n \ln \varepsilon \quad (4)$$

And let $\ln B + n \ln \varepsilon = y$, $\ln B = x$, by substituting it into Equation (3), we obtain

$$y = x + n \ln \varepsilon \quad (5)$$

Similarly, for the initial plastic strain moment ($\varepsilon = 0$) at different strain rates, i.e., Equation (2) becomes

$$\sigma = A \left(1 + C \ln \dot{\varepsilon}^*\right) \quad (6)$$

Immediately available

$$\sigma/A - 1 = C \ln \dot{\varepsilon}^* \quad (7)$$

By substituting $z = \sigma/A - 1$ into Equation (7), it can be obtained that

$$z = C \ln \dot{\varepsilon}^* \quad (8)$$

Therefore, the least squares method (LSM) for data processing of Equations (5) and (8) can ultimately determine parameters A , B , n , and C .

3.2. J–C Damage Model

According to the definition of the J–C damage model [7], considering the effects of stress triaxiality, strain rate, and temperature, the model parameters have clear meanings and can be determined through experiments. Therefore, it is widely used in many studies related to material failure and failure. The J–C model first defines damage as

$$D = \sum \frac{\Delta \varepsilon_p}{\varepsilon_f} \quad (9)$$

In the equation, D is the damage parameter factor, with a range of 0 to 1. At the beginning, $D = 0$. When $D = 1$, the material begins to fail. $\Delta \varepsilon_p$ is the plastic strain increment within a time step, and ε_f is the failure strain under the combined action of the current time-step stress state, strain rate, and temperature. The equivalent plastic strain expression at the beginning of the damage is as follows [7]

$$\varepsilon_f = [D_1 + D_2 \exp(D_3 \sigma^*)] \left(1 + D_4 \ln \dot{\varepsilon}^*\right) (1 + D_5 T^*) \quad (10)$$

Here D_1 – D_5 is the failure parameter of the material, while $\sigma^* = p_t / \sigma_{eff} = -\sigma_{kk} / \sigma_{eff} = -R_\sigma$, p_t is the pressure, σ_{eff} is the equivalent stress, R_σ is the stress triaxiality, $\dot{\epsilon}^* = \dot{\epsilon} / \dot{\epsilon}_0$ is the dimensionless plastic strain rate, $\dot{\epsilon}_0$ is the reference plastic strain rate, and T^* is the same as Equation (1).

For the damage model, Equation (9), the first term reflects the influence of stress triaxiality, which is expressed in exponential form and controlled by D_2 and D_3 . The equivalent plastic strain at the beginning of most material damage decreases with the increase of stress triaxiality, so a positive value, D_3 , is often taken. Compared with the commonly used equivalent strain failure rule, this model can reflect the effect of tensile and compressive stresses on material failure more effectively. The failure effect becomes smaller during tension, and the opposite is true: during compression, the failure strain is relatively large.

The second item reflects the influence of strain rate. Under the same stress state, the failure strain is linearly related to the logarithm of strain rate. By adjusting parameter D_4 , a practical relationship between strain rate and failure strain can be obtained.

The third item reflects the influence of temperature, and, at the same strain rate, the failure strain is linearly related to dimensionless temperature.

4. Collision Finite Element Model

This article applies the Lagrange method [25,26] in the finite element simulation analysis of simulated collision processes, which applies the material J–C constitutive and damage failure models discussed in the previous section to the high-speed collision process, fully considering the collision contact boundary and energy loss.

According to the simplified model of the second water-saving collision problem—the model of square plates being impacted by bullets, and for the study of PMMA square plates being impacted by bullets—Kazarinov [14] studied the impact test and numerical simulation (in LS-DYNA) of this problem in an air environment, and tested PMMA plate size: $a = b = 100$ mm, $h = 4$ mm~10 mm; and bullet size: $d = 6$ mm and $l = 20$ mm, as shown in Figure 1. The mechanical and physical properties of PMMA sheets and steel bullet materials are shown in Table 1.

Table 1. Material properties used in numerical model [14].

	PMMA Target	Steel Projectile
Young's modulus, E (MPa)	3300	2.09×10^5
Poisson's ratio, μ	0.35	0.28
Density, ρ (kg/m ³)	1180	7720
Ultimate tensile stress, σ_c (MPa)	7240	
Ultimate tensile intensity factor, K_{Jc} (MPa)	1.7	
Failure displacement [23]	0.011	

Therefore, in order to verify the accuracy of the impact method based on the J–C constitutive and damage failure models constructed in this article, a finite element model with corresponding geometric dimensions [14] was established based on the ABAQUS platform, in order to obtain explicit analysis. Furthermore, three-dimensional solid elements were selected, and the local division of the finite element model mesh and the overall model are shown in Figure 2. In order to simulate the damage and fracture of materials in the impact area better, the central element mesh of the square plate is meshed finely. In finite element simulation research, the boundary constraint conditions of PMMA board are shown in Table 2. Compared with PMMA plates, bullets are rigid bodies with only axial degrees of freedom (velocity) perpendicular to the plane direction of the plate.

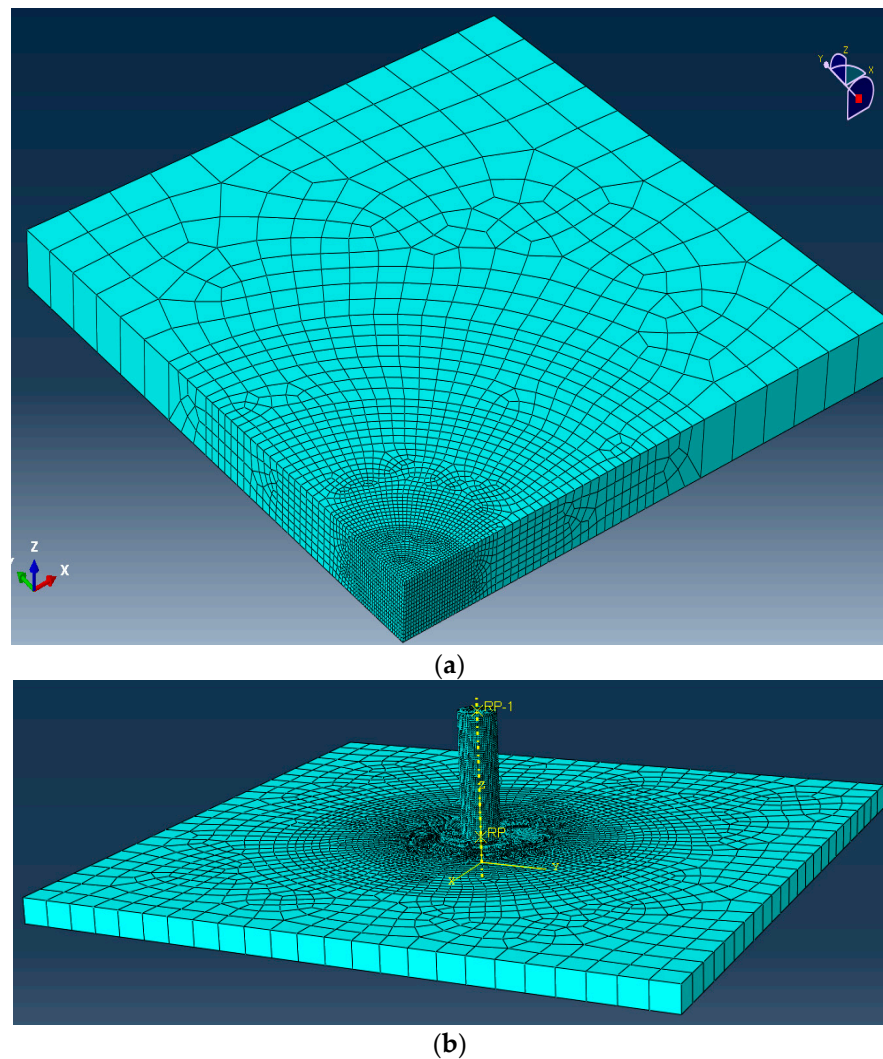


Figure 2. PMMA impact model and mesh generation. (a) Local mesh (a quarter part). (b) Finite element overall model.

Table 2. Boundary conditions used in numerical model.

Position	Boundary State
$x = -a/2$	$u_x = u_y = u_z = \gamma_x = \gamma_y = \gamma_z = 0$
$y = -b/2$	$u_x = u_y = u_z = \gamma_x = \gamma_y = \gamma_z = 0$
$x = a/2$	$u_z = \gamma_x = 0$
$y = b/2$	$u_z = \gamma_y = 0$

5. Verification of Collision Finite Element Method (CFEM)

Based on the J–C constitutive and damage failure models mentioned above, this article uses LSM to determine the parameters of the material based on experimental data, and compares the correctness of the analysis methods and parameters. The finite element impact process analysis of the square plate finite element model is also verified.

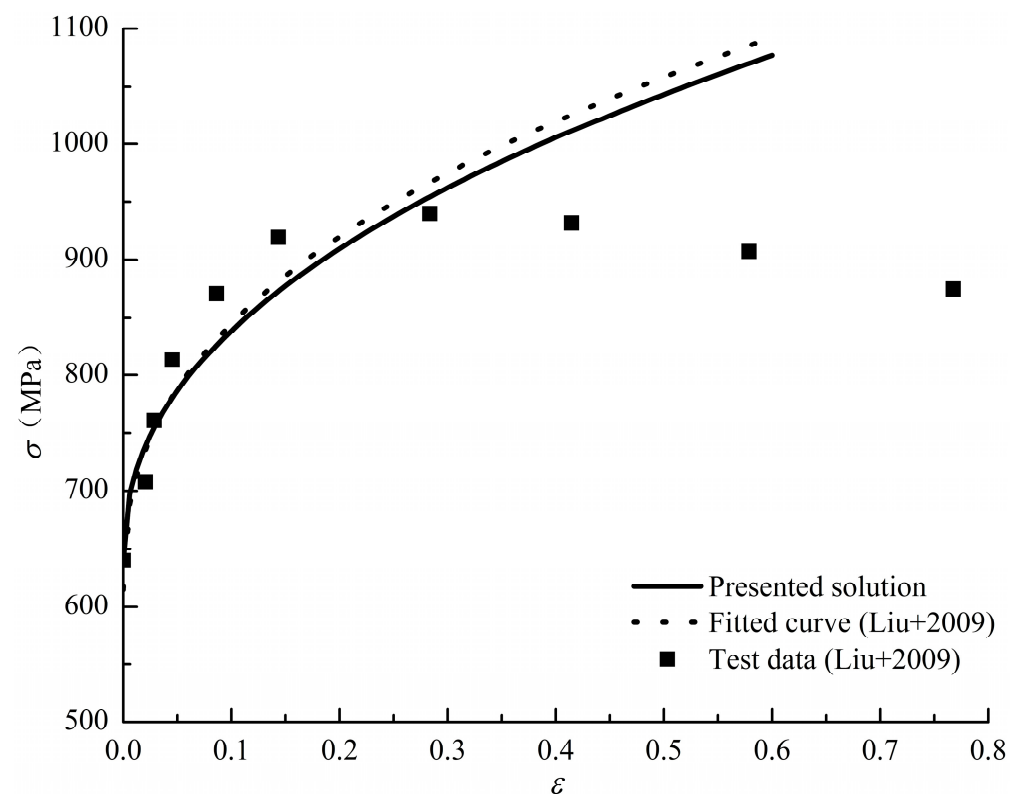
5.1. Verification and Parameter Determination of J–C Constitutive Model

In order to verify the accuracy of the J–C constitutive model and the presented LSM parameter determination method, this paper firstly obtains the parameters of the J–C constitutive equation by normalizing the tensile test data of 50SiMnVB steel at different strain rates, and, through the theory and data processing analysis in Section 3, as shown in Table 3, the model parameters corresponding to the strain rate of 10^{-3} s^{-1} are given.

Table 3. Parameter determination of the J–C constitutive model for steel and PMMA.

Material		<i>A</i>	<i>B</i>	<i>n</i>	<i>C</i>
50SiMnVB steel	reference [8]	615	588	0.408	0.034
	Presented J–C model	640	547	0.439	0.033
PMMA	Presented J–C model	55	312.78	0.62	0.105

By testing SHPB at different strain rates, Liu [8] obtained quasi-static and dynamic curves of normalized 50SiMnVB steel at room temperature, and carried out the J–C model parameters by fixing the strain rate and fitting coefficient from test curves, shown as Figure 3. Then, in this paper, the presented LSM is carried out to confirm the J–C model parameters, as seen in Table 3 and Figure 3.

**Figure 3.** Steel J–C constitutive model verification ($\dot{\epsilon} = 10^{-3} \text{ s}^{-1}$) [8].

Similarly, for the PMMA compression test data [13], the corresponding J–C constitutive model parameters can be obtained, as shown in Table 3 and Figure 4. From the figure, it can be seen that the J–C model has a good fit with the experimental values, especially in the initial stage of plastic strain.

Due to the varying speed of strain changes during the process of structural breakdown during impact, the strain rate varies. Therefore, for PMMA materials with different strain rates, the J–C model was compared and analyzed with experimental values, as shown in Figure 5. As shown in the figure, for PMMA materials, the J–C model can characterize the plastic or viscoelastic properties of the material within a certain range under different strain rates, with good accuracy.

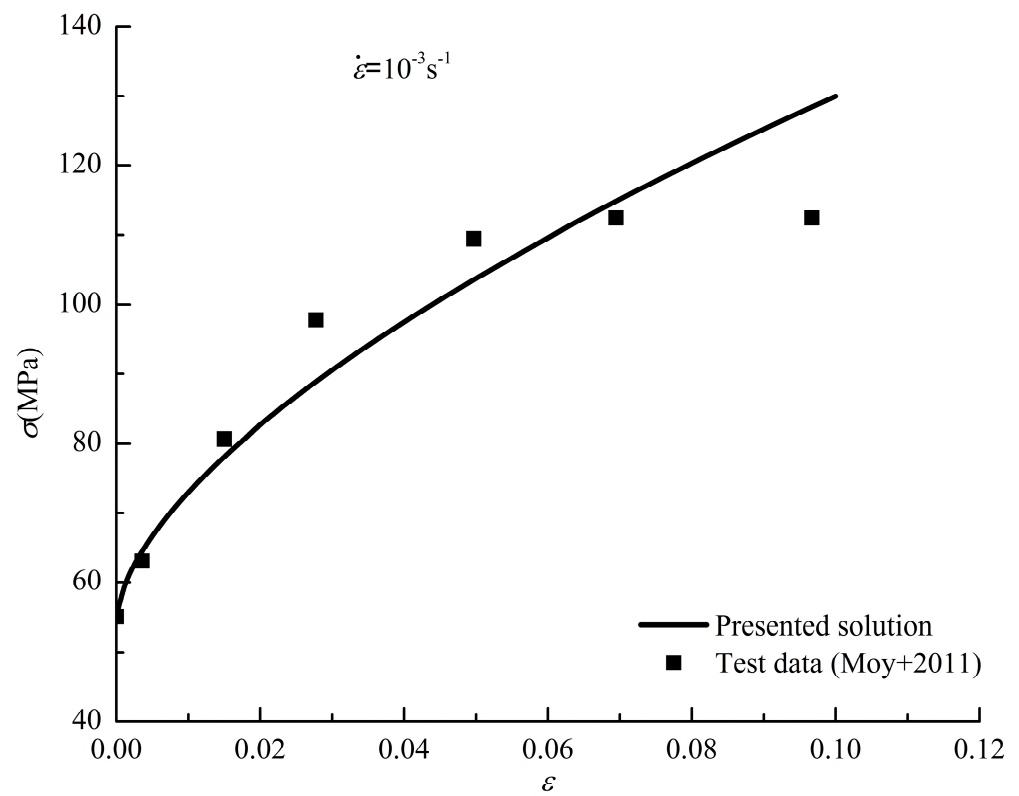


Figure 4. PMMA J-C constitutive model verification ($\dot{\epsilon} = 10^{-3} \text{ s}^{-1}$) [13].

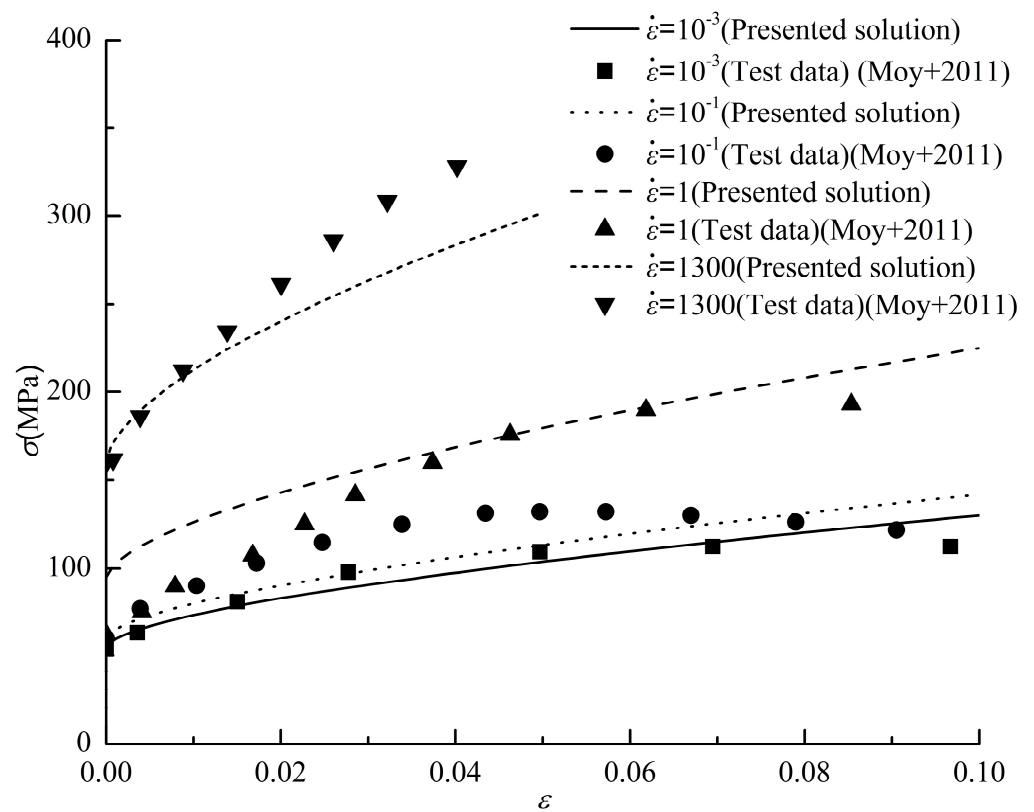


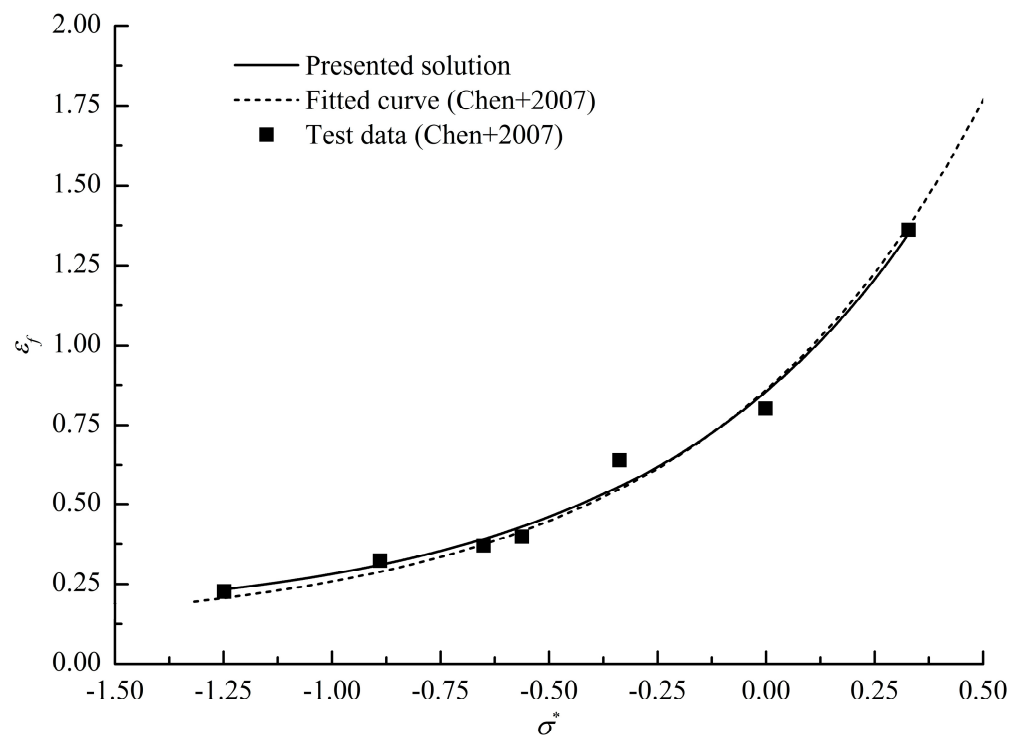
Figure 5. PMMA J-C constitutive model verification for different strain rates [13].

5.2. Verification and Parameter Determination of J–C Constitutive Model

For the J–C damage failure model, this paper uses the previous least squares method to determine the parameters of the J–C damage failure model from the quasi-static mechanical property experiment and compression SHPB experiment data of material specimens under different stress states and temperatures; that is, D_1 , D_2 , and D_3 are determined from the quasi-static triaxial stress fracture test, and D_4 and D_5 are determined from the fracture test under different strain rates and temperatures. The J–C damage failure model parameters of 45 steel obtained in this article are shown in Table 3.

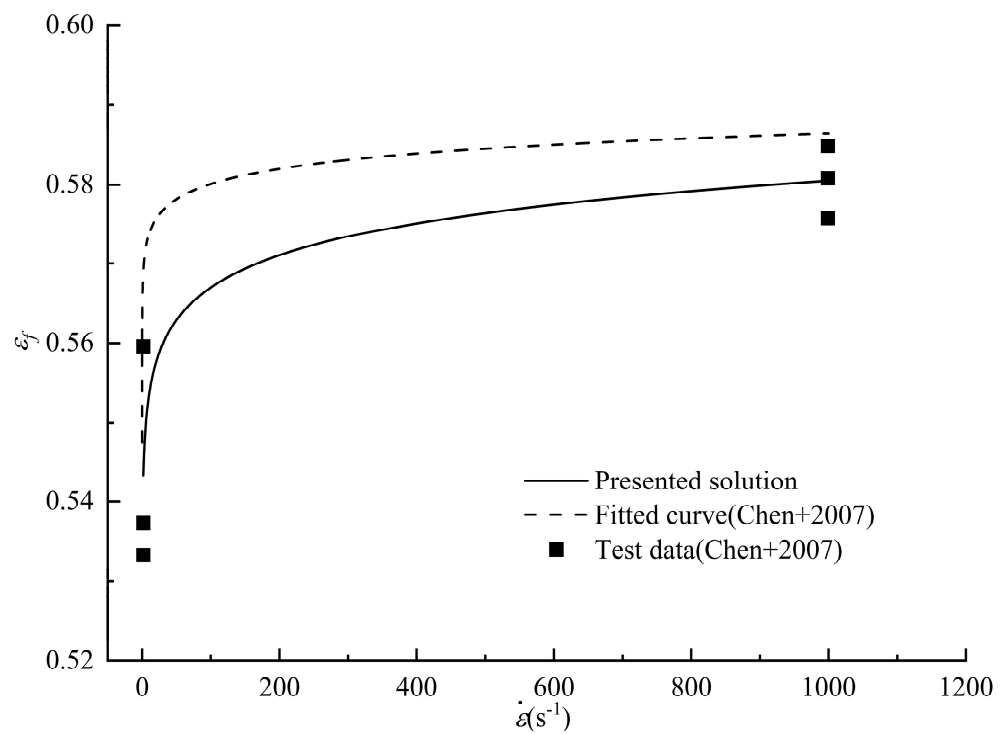
From Table 3, it can be seen that the parameters determined by the least squares method in this article are basically consistent with the literature values. At the same time, based on the parameters and experimental data determined in this article, a comparative analysis was conducted on the J–C damage failure model and experimental data of 45 steel, as shown in Figures 6–8. From the figures, it can be seen that the J–C damage model has a good agreement with the experimental values.

Similarly, according to the above methods, the quasi-static tensile testing and compression test [11,20] of a smooth round bar at room temperature, the quasi-static tensile testing of a smooth round bar at different temperatures, and the tensile testing of a smooth round bar at different strain rates and other test data were processed, and the J–C damage failure model parameters of PMMA materials were finally determined. The specific parameter values are shown in Table 3.

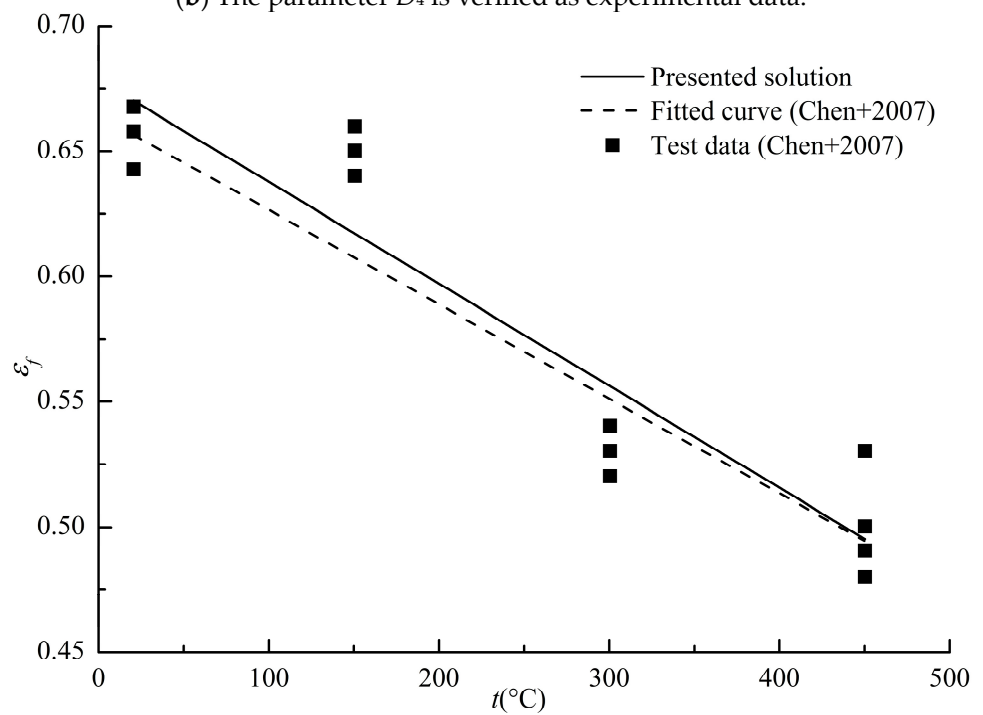


(a) The parameters D_1 , D_2 , and D_3 are verified as experimental data.

Figure 6. Cont.



(b) The parameter D_4 is verified as experimental data.



(c) The parameter D_5 is verified as experimental data.

Figure 6. Steel 45 J–C constitutive and failure model parameters [16].

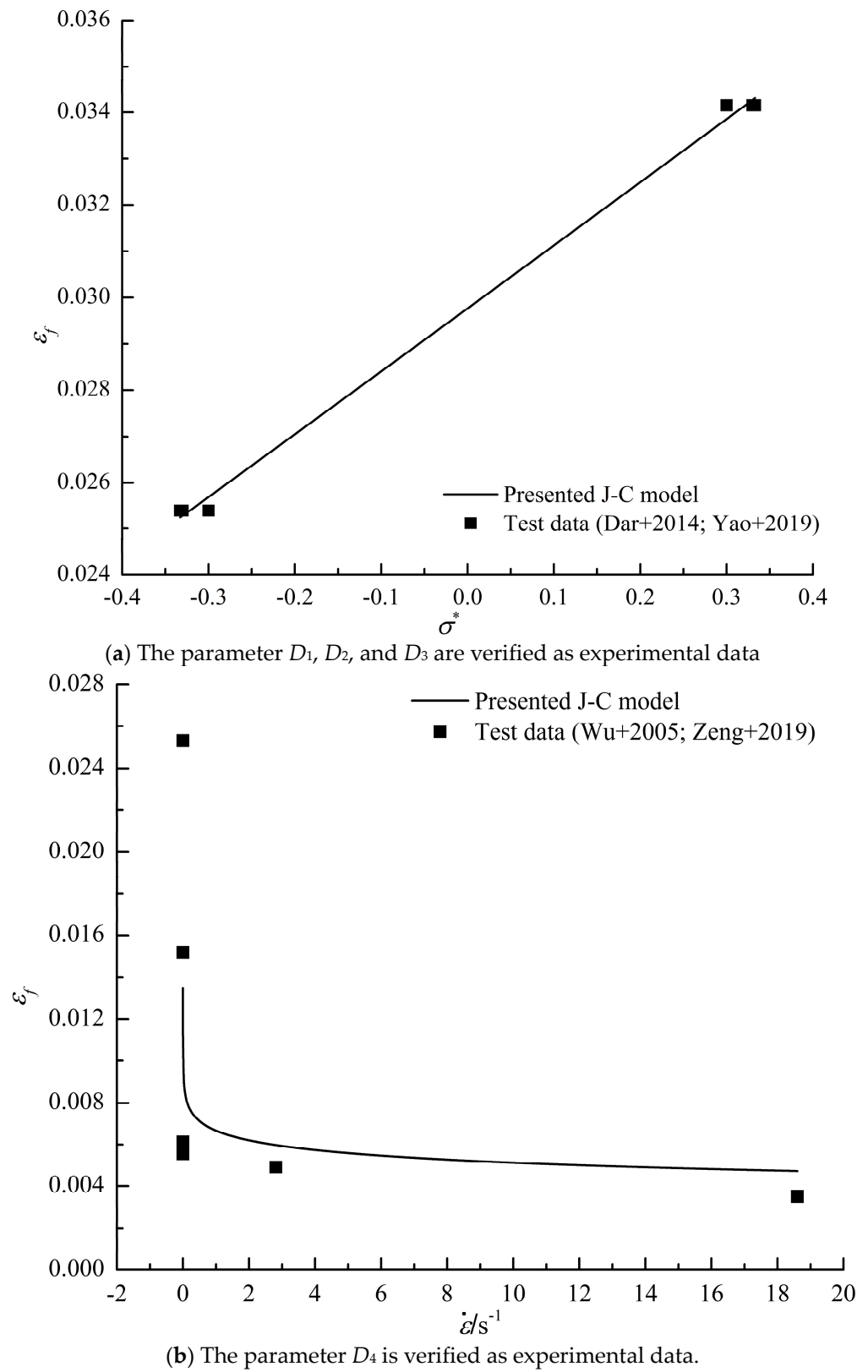
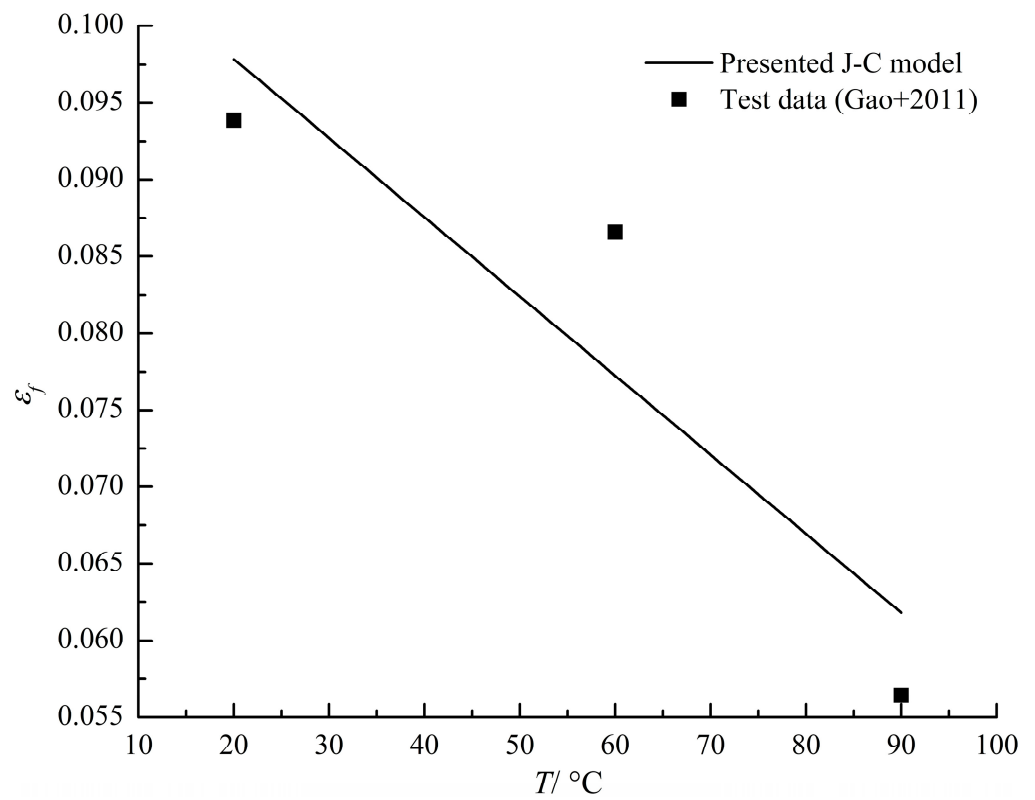


Figure 7. Cont.



(c) The parameter D_5 is verified as experimental data.

Figure 7. PMMA J-C constitutive and failure model parameters [11,15,18,20,21].

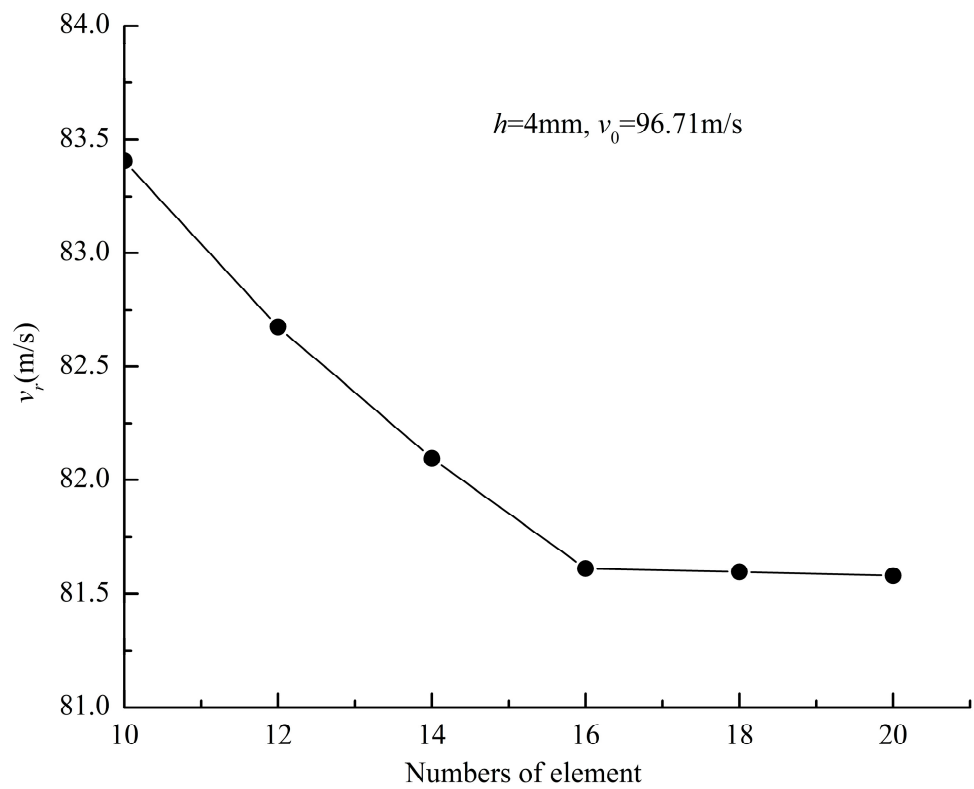


Figure 8. Convergence of numerical method.

5.3. Experimental Verification of Collision Numerical Simulation Method

The J–C constitutive model and damage failure model parameters of PMMA are established through the previous section. The finite element modeling is carried out for the test block, with $h = 4$ mm. The entire impact process and the residual velocity of the bullet, v_r , can be calculated by applying the boundary constraints of the plate (see Figure 1 and Table 2) and the initial condition, v_0 , of the bullet.

It is noted that the element mesh density would affect numerical results in finite element analysis. Figure 8 shows that the residual velocity of the bullet varies from element numbers in thickness at the center of the block, which means that the presented numerical method has a good convergence when the element numbers in thickness are larger than 16. So, in the following impact analysis, the model has been meshed densely to guarantee its convergence.

Figure 9 shows a comparison between the numerical simulation calculation of the damage caused by the bullet, $v_0 = 70$ m/s, impacting and penetrating the PMMA plate ($h = 10$ mm) and the test [14]. From Figure 9, it can be seen that the finite element simulation calculation and test damage show a cross cracking with four major fractures, although test results had one more fracture than those in simulation.

Figure 10 shows the relationship between the initial velocity and residual velocity of bullets penetrating PMMA plates of different thicknesses, and compares them with the numerical solutions and experimental values in the literature [14]. From Figure 10, it can be seen that the calculation results of the finite element method based on the J–C constitutive and damage models constructed in this article are in good agreement with the experimental results. For the block with $h = 4$ mm, the presented numerical results are almost the same as test and reference [14] data, seen as Figure 10a, while, for the block with $h = 10$ mm, the presented numerical results are little bigger than the test data and the reference [14] data are smaller. The major reason is material property uniformity, which would affect the parameter deviation of the J–C model.

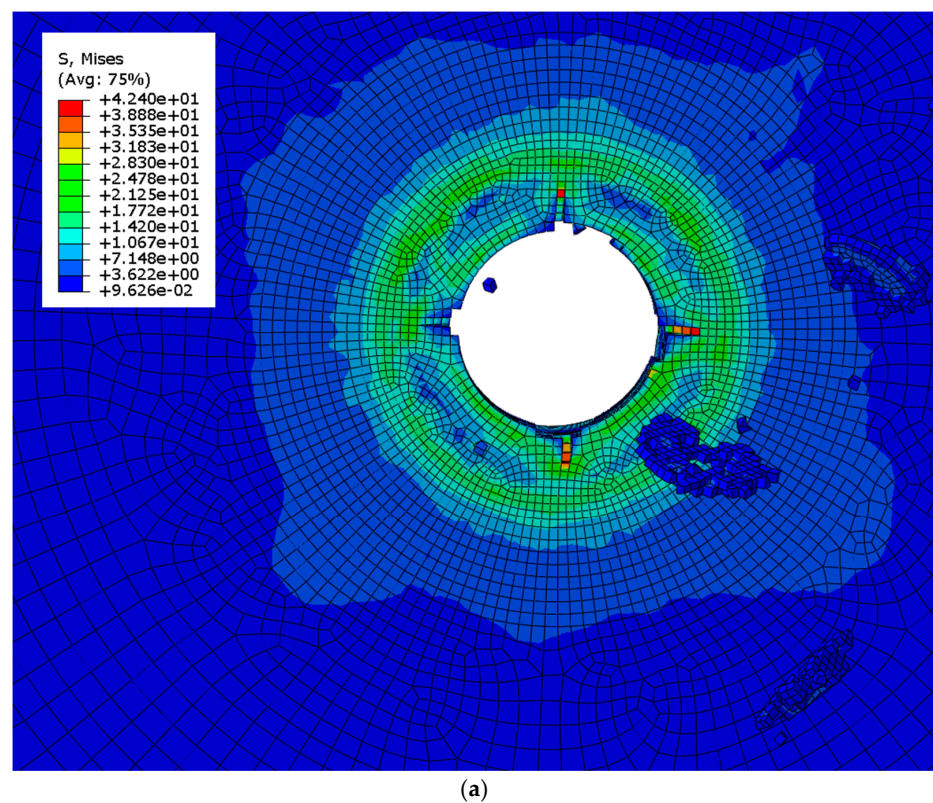


Figure 9. Cont.

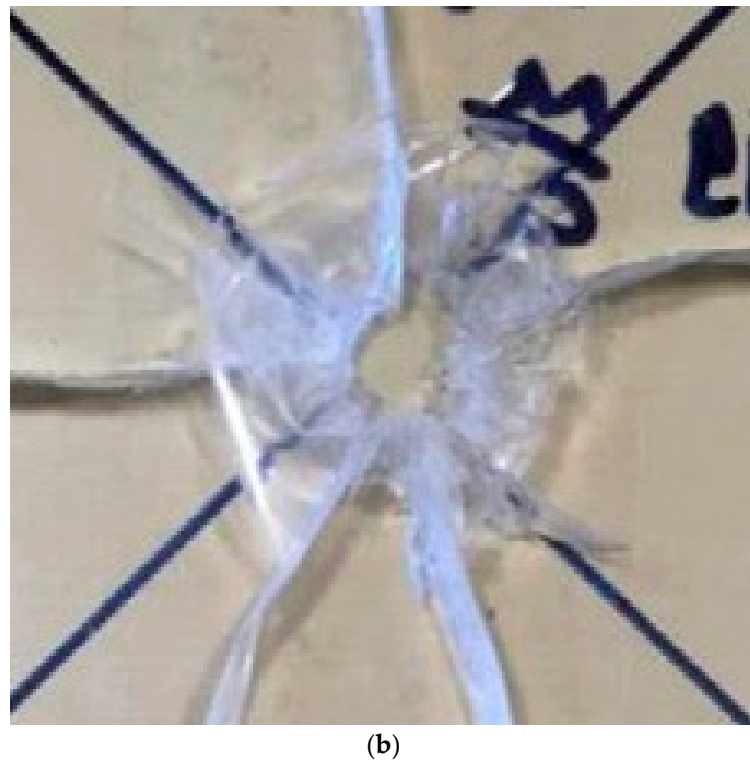


Figure 9. Fracture patterns: experiment and numerical simulation. (a) Numerical simulation fracture pattern; and (b) experiment fracture pattern [14].

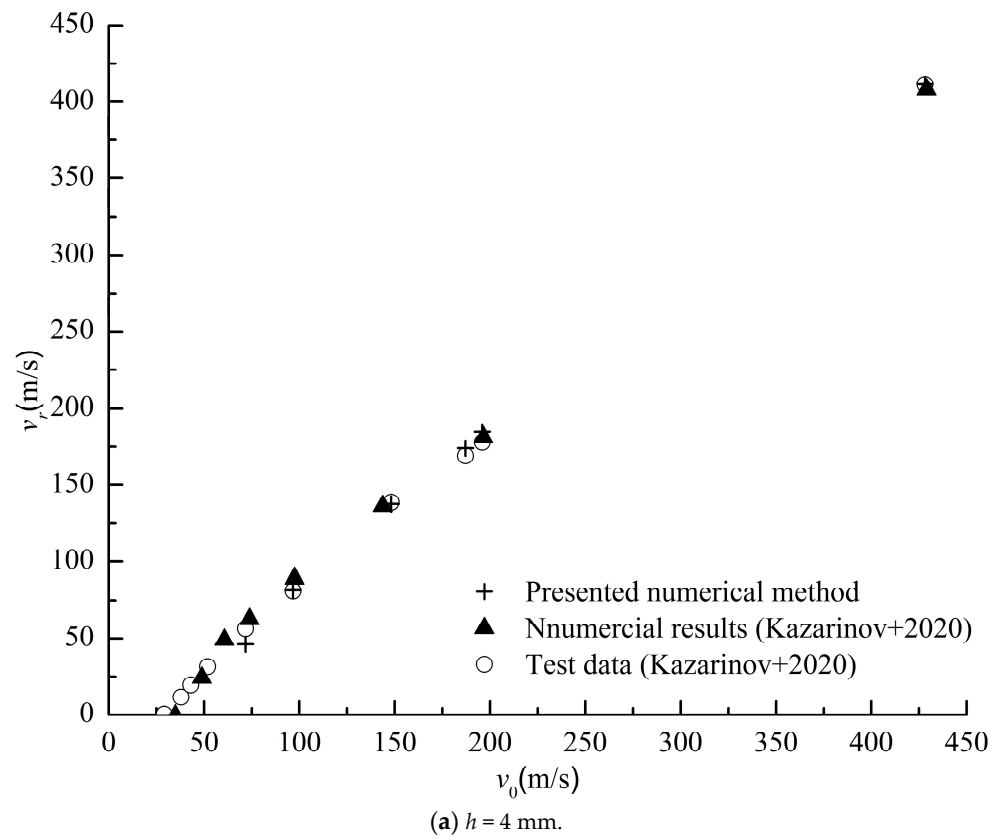


Figure 10. Cont.

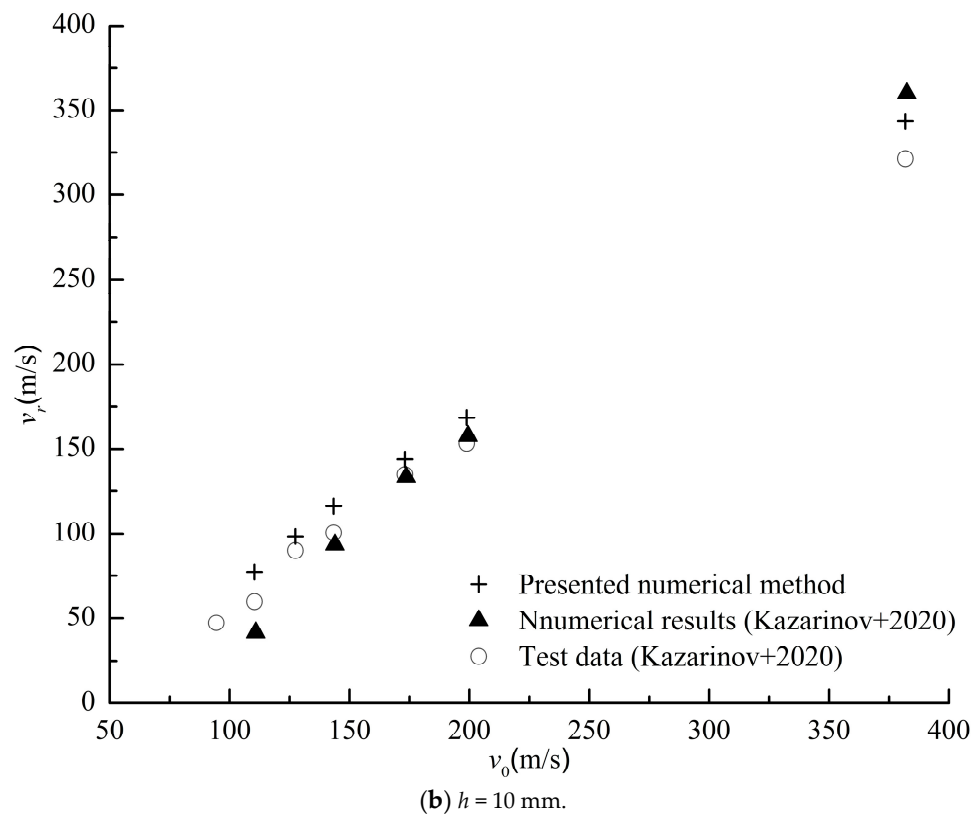


Figure 10. Residual velocity—initial velocity dependencies for different specimen thicknesses [14].

Therefore, the analysis results indicate the rationality and accuracy of the numerical simulation calculation method constructed in this paper.

6. Impact Analysis of PMMA Plate under Pressure

For the problem of underwater penetration by concentrated loads, based on the simplification of the previous section, this paper studies the problem of plate penetration by concentrated loads. According to the shell theory, the internal stress, σ , of the spherical structure of a carrier or deep submersible under external uniform pressure is

$$\sigma = \frac{pD}{2h} \tag{11}$$

Here p , D , and h are shown in Figure 1.

Therefore, in order to consider the response of external pressure and simulate the membrane stress state of underwater pressure-resistant spherical shells, in the simplified finite element simulation calculation of the plate structure in the previous section, the surface pressure, p , effect of the square plate will be added here, and, in addition to applying displacement constraints on the boundary, internal force stress boundary conditions still need to be added; that is, in Table 2, the compressive stress, σ_x , is added at $x = a/2$ as a force boundary.

$$\sigma_x = \sigma = \frac{pD}{2h} \tag{12}$$

And at $y = b/2$, adding the compressive stress, σ_y , as a force boundary

$$\sigma_y = \sigma = \frac{pD}{2h} \tag{13}$$

To increase comparability, the size of the PMMA square plate in the previous section was applied to the deep-sea spherical transparent glass structure, $D = 2000$ mm. A finite

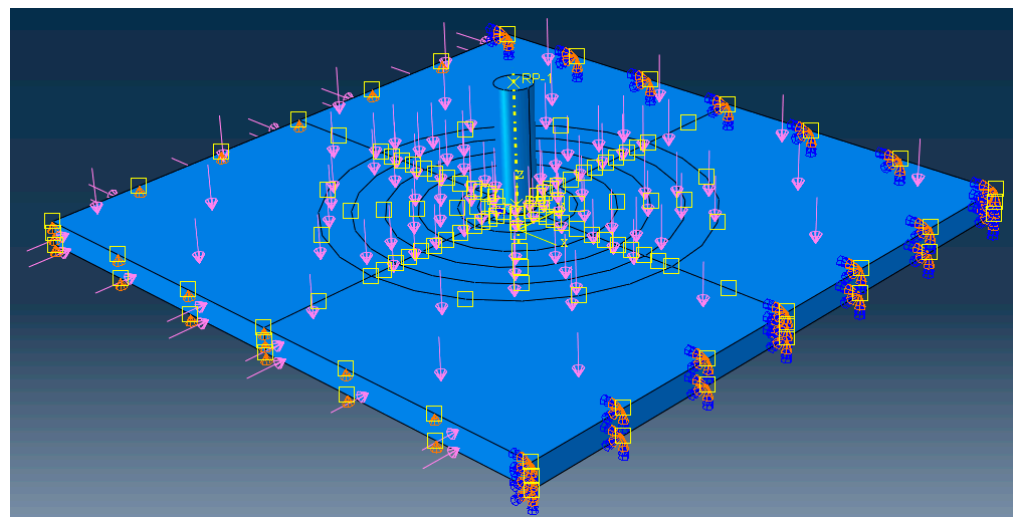
element model was constructed, and impact dynamics calculations were conducted by integrating the J–C constitutive and damage failure models. Finally, the dynamic response of the PMMA square plate under pressure to bullet impact penetration was obtained.

Figure 11a shows the loadings and boundary of the finite element model. After dynamic numerical analysis, Figure 11b proposes the deformation contour of the PMMA plate after impacting, while Figure 11c shows the equivalent stress contour and damage situation of the PMMA plate after bullet impact penetration. From these figures, it can be obviously seen that, due to external pressure, the PMMA block is more severely damaged than that under no pressure (seen as Figure 9a).

Figure 12 shows the residual velocity of a bullet with an initial velocity of $v_0 = 200$ m/s under different pressures penetrating PMMA square plates with different thicknesses. From this figure, it can be found that, as the external pressure increases, the residual velocity of the bullet also increases, which indicates that the square plate PMMA structure reduces its impact resistance to bullet penetration due to its resistance to the pressure loading.

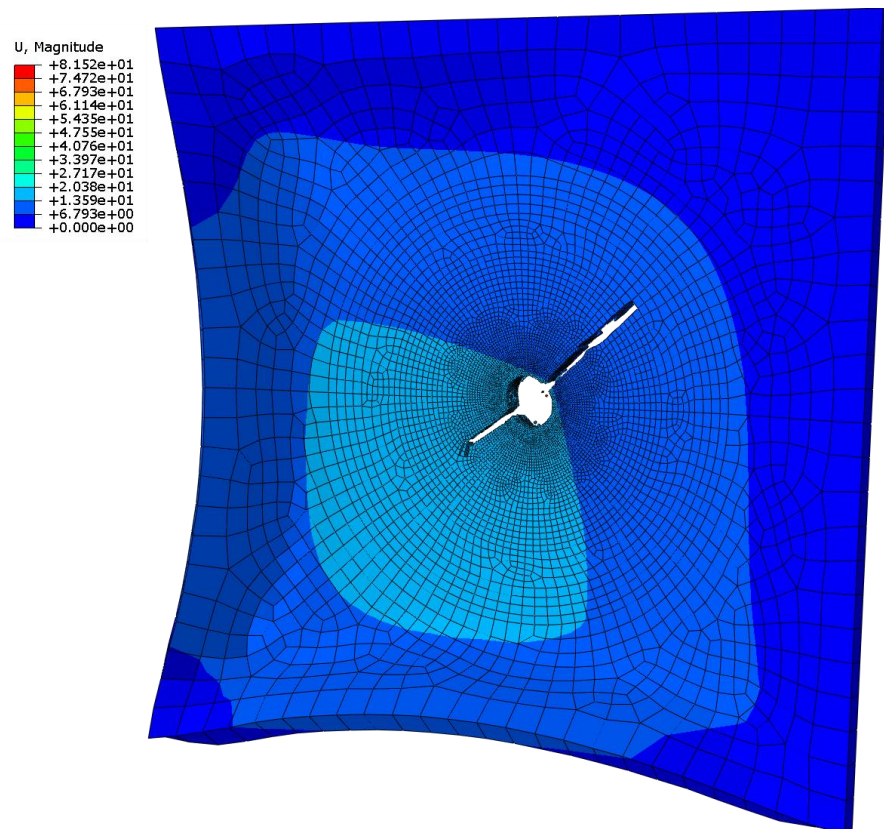
Moreover, the residual velocity of three different thicknesses of PMMA plates under bullet impact penetration with initial velocity $v_0 = 200$ m/s was studied as a function of external pressure, as shown in Figure 13. As shown in the figure, when the external pressure increases, the residual velocity will increase too, and, as the thickness of the plate increases, the residual velocity increases more severely. The effect of surface external pressure on the thick plate is more obvious.

For the structural damage deformation and strain caused by bullet impact penetration on the PMMA block, Figure 14 shows the variation history of the structural deformation and plastic strain at different positions during the impact penetration process of the PMMA board with $h = 4$ mm over time. From these figures, it can be seen obviously that the plastic strain caused by tearing damage at the edge of the hole is relatively large, even greater than the plastic strain at the center of the hole that was knocked out as a whole; the plastic strain in the area far from the bullet hole appears later and is numerically smaller.

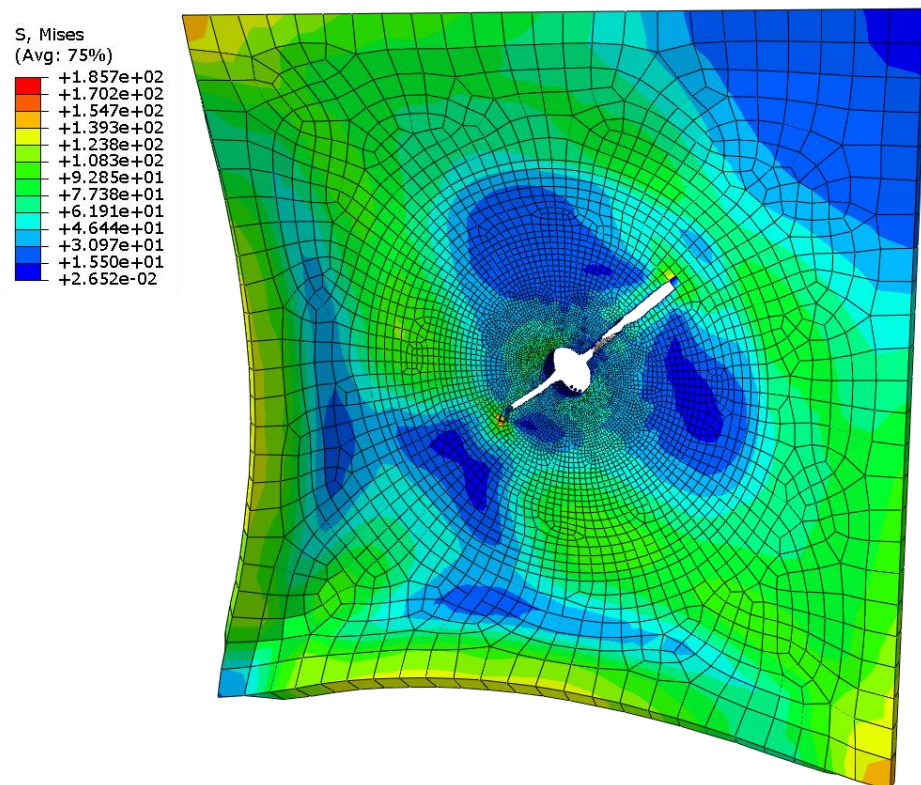


(a) Finite element overall model with loading and boundary.

Figure 11. Cont.



(b) Deformation contour of PMMA block after impacting ($t = 0.336$ ms).



(c) VonMises stress contour of PMMA block after impacting ($t = 0.336$ ms).

Figure 11. The loading, boundary, and deformation and stress contour in FEM.

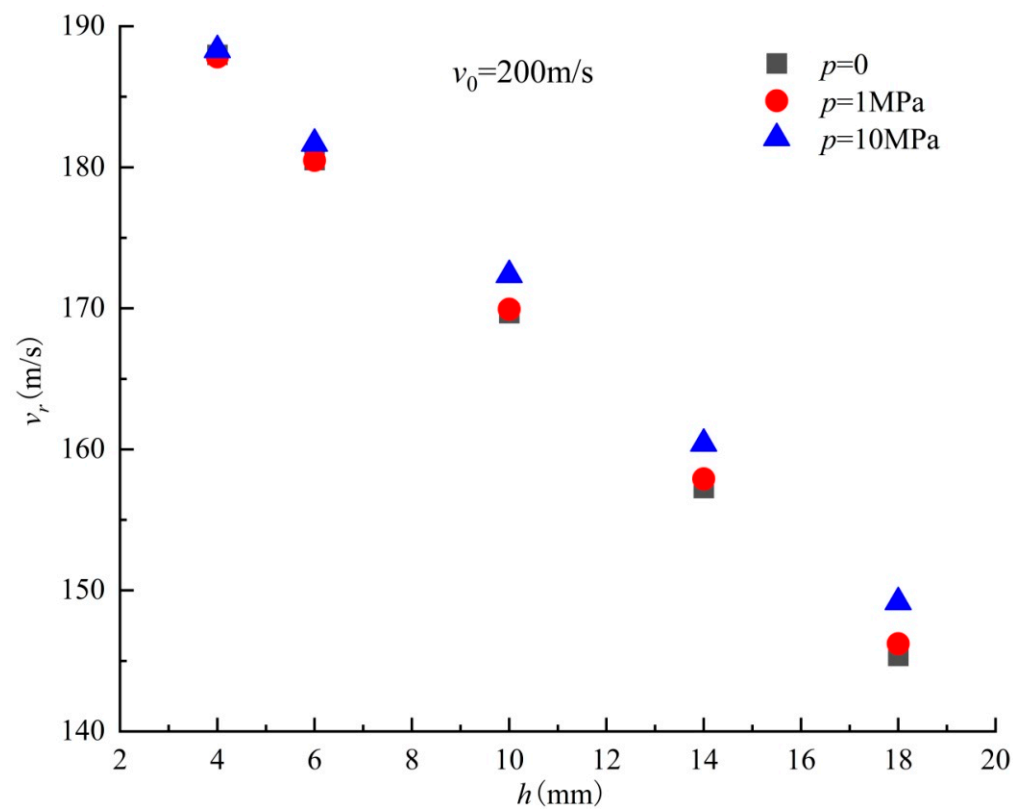


Figure 12. Residual velocity—specimen thickness dependencies for different pressures.

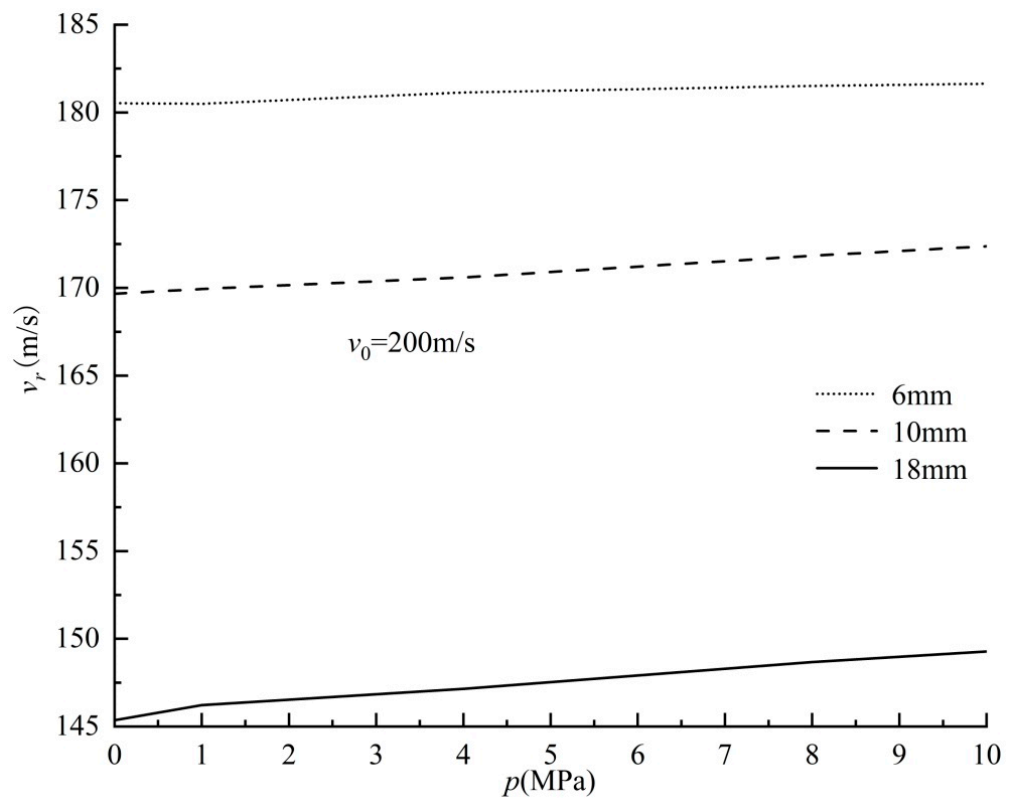


Figure 13. Residual velocity—pressure dependencies for different specimen thicknesses.

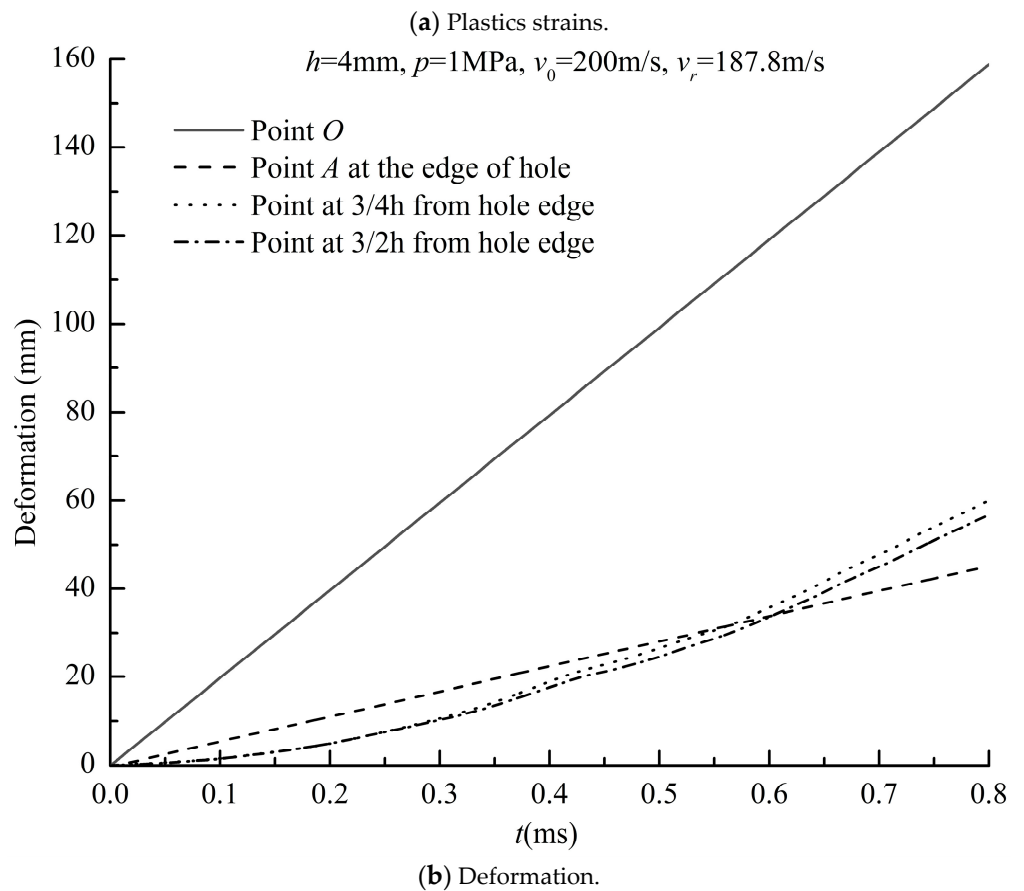
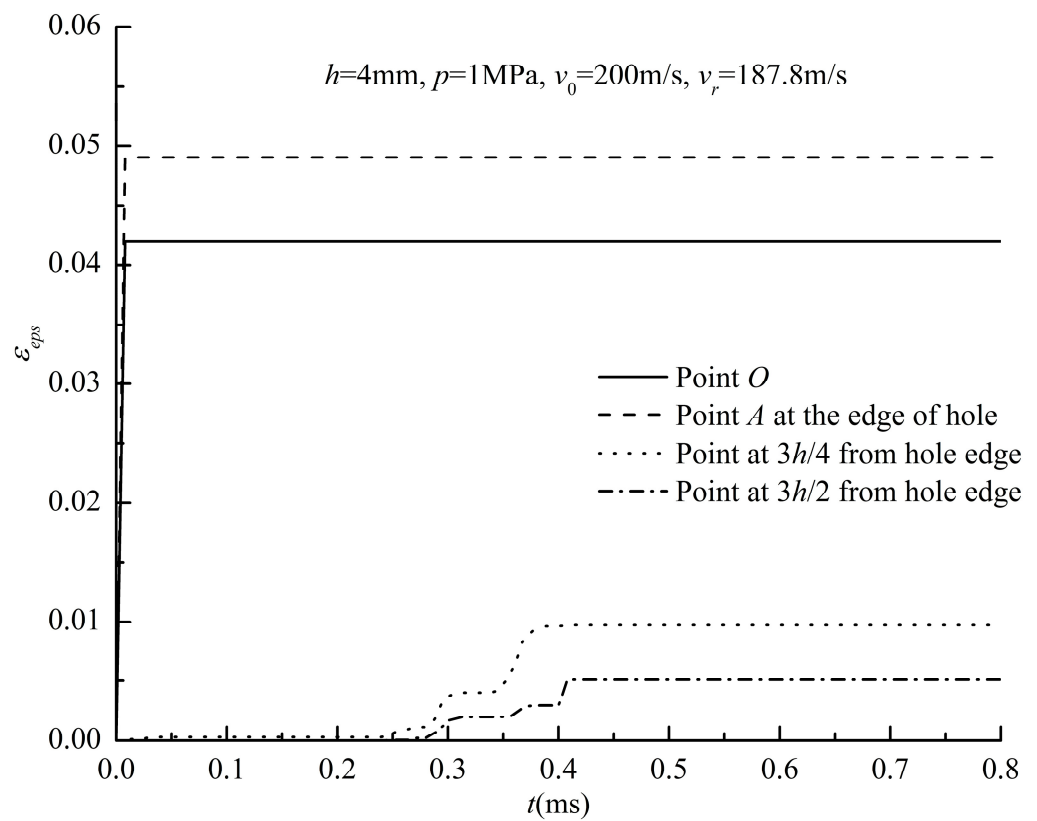


Figure 14. Plastics strains and deformation vary from time at different positions.

7. Summary and Conclusions

In this paper, based on the J–C constitutive and damage models, a finite element calculation model for collision is built, and the parameters of the J–C model are verified using different materials. After verification using the test of bullet impacting a PMMA plate, a simplified model was constructed for the dynamic analysis of a spherical hull under concentrated impact loadings in the underwater state, and series of numerical calculations were carried out accordingly. The main findings of the article are as follows:

(1) The least squares method (LSM) is developed to determinate the parameters of the J–C constitutive and damage models. After comparing with test data and reference [8] results, respectively, the presented LSM was confirmed and also applied to determinate PMMA materials in the J–C model at different strain rates.

(2) Based on the J–C constitutive and damage models, a numerical model of plate with bullet impacting is obtained on Abaqus software. Moreover, for different thicknesses of plates and initial velocities of bullets, the presented numerical results with the J–C model could have a good agreement with test data and even with numerical results from LS-DYNA.

(3) From the theory of plate and shell, a plate with bullet impact is simplified to simulate the spherical hull under impact loading. The numerical results show that the residual velocity with pressure is larger than that without pressure, and it also raises when the pressure increases. Deformation of the impacted block is larger and more serious too. Such a pressure effect will be more obvious for the thick plate.

Author Contributions: Conceptualization, methodology, writing-review and editing, resources, supervision, project administration, funding acquisition, Q.D.; software, validation, formal analysis, investigation, writing—original draft preparation, F.L.; data curation and visualization, Q.L. All authors have read and agreed to the published version of the manuscript.

Funding: This research was funded by the National Key R&D Program-Special Deep Sea Key Technology and Equipment ‘Damage Detection and Prediction of Glass Ball Cabin’ (grant number 2018YFC0308004), and Program of National Natural Science Foundation of China ‘Theoretical and Experimental Research about Structure of Pressure Toroidal Shell in Underwater Engineering’ (grant number 51109190).

Institutional Review Board Statement: Not applicable.

Informed Consent Statement: Not applicable.

Data Availability Statement: Not applicable.

Conflicts of Interest: The authors declare no conflict of interest.

References

1. Ali, U.; Karim, K.J.B.A.; Buang, N.A. A review of the properties and applications of Poly (Methyl Methacrylate) (PMMA). *Polym. Rev.* **2015**, *55*, 678–705. [[CrossRef](#)]
2. Kohnen, W. Manned underwater vehicles 2017–2018 global industry overview. *Mar. Technol. Soc. J.* **2018**, *52*, 125–151. [[CrossRef](#)]
3. Du, Q.H.; Hu, Y.; Cui, W.C. Safety assessment of the acrylic conical frustum viewport structure for a deep sea manned submersible. *Ships Offshore Struct.* **2016**, *12* (Suppl. S1), 221–229. [[CrossRef](#)]
4. Du, Q.H.; Jiang, H.G.; Hu, X.K. Creep behavior analysis of conical observation window for human occupied vehicle based on ABAQUS. *Chin. J. Ship Res.* **2022**, *17*, 108–116.
5. Kemper, B.; Gross, L. Developing “design by analysis” methodology for windows for pressure vessels for human occupancy. *ASCE-ASME J. Risk Uncertain. Eng. Syst. Part B Mech. Eng.* **2020**, *6*, 30906. [[CrossRef](#)]
6. Du, Q.H.; Xu, D.H.; Liu, D. Experimental and numerical analysis on pressure effect of polymethyl methacrylate (PMMA) structure in electric-resistance strain measurement. *Ships Offshore Struct.* **2022**, *17*, 2001–2011. [[CrossRef](#)]
7. Johnson, G.R.; Cook, W.H. Fracture characteristics of three metals subjected to various strains, strain rates, temperatures and pressures. *Eng. Fract. Mech.* **1985**, *21*, 31–48. [[CrossRef](#)]
8. Liu, P.P.; Yin, Y.; Chang, L.Z.H.; Xie, Y. Establishing of Johnson-Cook constitutive equation for normalized steel 50SiMnVB. *Ordinance Mater. Sci. Eng.* **2009**, *32*, 45–49.
9. Guo, Z.T.; Gao, B.; Guo, Z.; Zhang, W. Dynamic constitutive relation based on J–C model of Q235 steel. *Explos. Shock. Waves* **2018**, *38*, 804–810.

10. Yu, P.; Yao, X.H.; Han, Q.; Zhang, S.G.; Li, Z.Q. Dynamic constitutive model of PMMA at room temperature. *Explos. Shock. Waves* **2013**, *33* (Suppl. S1), 88–91.
11. Yao, H.Q.; Yang, P.Y.; Liu, X.; Qu, J. Compression mechanical properties of PMMA under room temperature at low and high strain rates. *Earthq. Eng. Eng. Dyn.* **2019**, *39*, 91–96.
12. Wang, Z.Y.; Wang, Y.Q.; Du, X.X.; Zhang, T.X.; Yuan, H.X. Quasi-static tensile test of thick acrylic sheets at different temperatures. *J. Southeast Univ. Nat. Sci. Ed.* **2018**, *48*, 132–137.
13. Moy, P.; Gunnarsson, C.A.; Weerasooriya, T.; Chen, W. Stress-strain response of PMMA as a function of strain-rate and temperature. *Dyn. Behav. Mater.* **2011**, *1*, 125–133.
14. Kazarinov, N.A.; Bratov, V.A.; Morozov, N.F.; Petrov, Y.V.; Balandin, V.V.; Iqbal, M.A.; Gupta, N.K. Experimental and numerical analysis of PMMA impact fracture. *Int. J. Impact Eng.* **2020**, *143*, 103597. [[CrossRef](#)]
15. Wu, H.Y.; Ma, G.; Xia, Y.M. Experimental study on mechanical properties of PMMA under unidirectional tensile at low and intermediate strain rates. *Int. J. Impact Eng.* **2005**, *20*, 193–199.
16. Chen, G.; Chen, Z.F.; Xu, W.F.; Chen, Y.M.; Huang, X.C. Investigation on the J–C ductile fracture parameters of 45 steel. *Explos. Shock Waves* **2007**, *27*, 131–135.
17. Shash, N.; Zuzov, V.N. Modified Johnson–Cook model-based numerical simulation of small arms bullets penetration in the Aluminum alloy plates. *Sci. Educ. Bauman MSTU* **2017**, *1*, 1–19. [[CrossRef](#)]
18. Zeng, G.W.; Liu, H.X.; Shen, G.J.; Wu, L. Experimental research on viscoelastic damage constitutive model of PMMA. *J. Mater. Sci. Eng.* **2019**, *37*, 801–805.
19. Klosak, M.; Rusinek, A.; Jankowiak, T.; Qoubba, Z.E.; Boumbimba, R.M.; Bendarma, A. Dynamic perforation and compression tests of PMMA for a wide range of temperatures—Experimental and preliminary numerical analysis. *EPJ Web Conf.* **2018**, *183*, 2055. [[CrossRef](#)]
20. Dar, U.A. Numerical characterization of acrylic polymer under quasi-Static and dynamic loading by implementing viscoelastic material model. *Compos. Mech. Comput. Appl. Int. J.* **2014**, *5*, 195–205. [[CrossRef](#)]
21. Gao, Z.Z.; Liu, Z.Q.; Liu, W.; Yue, Z.F. Experimental and constitutive investigation on tensile and compressive behavior of MDYB-3 at different temperatures and loading rates. *Int. J. Polym. Mater. Polym. Biomater.* **2011**, *60*, 340–350. [[CrossRef](#)]
22. Forquin, P.; Nasraoui, M.; Rusinek, A.; Siad, L. Experimental study of the confined behaviour of PMMA under quasi-static and dynamic loadings. *Int. J. Impact Eng.* **2012**, *40–41*, 46–57. [[CrossRef](#)]
23. Varela-Rizo, H.; Weisenberger, M.; Bortz, D.R.; Martin-Gullon, I. Fracture toughness and creep performance of PMMA composites containing micro and nanosized carbon filaments. *Compos. Sci. Technol.* **2010**, *70*, 1189–1195. [[CrossRef](#)]
24. Tioshenko, S.; Woinowsky-Krieger, S. *Theory of Plates and Shells*; McGraw-Hill Book Company, Inc.: New York, NY, USA, 1959.
25. Chung Kim Yuen, S.; Nurick, G.N.; Langdon, G.S.; Iyer, Y. Deformation of thin plates subjected to impulsive load: Part III—An update 25 years on. *Int. J. Impact Eng.* **2017**, *107*, 108–117. [[CrossRef](#)]
26. Wang, F. Study of Finite Element Method and Application for High Velocity Impact. Ph.D. Dissertation, University of Science and Technology of China, Hefei, China, May 2007.

Disclaimer/Publisher’s Note: The statements, opinions and data contained in all publications are solely those of the individual author(s) and contributor(s) and not of MDPI and/or the editor(s). MDPI and/or the editor(s) disclaim responsibility for any injury to people or property resulting from any ideas, methods, instructions or products referred to in the content.